Monocyte Metabolic Plasticity and Cytokine Production Differentiate Latent TB Infection from Active Disease

Running title: Monocyte Metabolism and Function in Latent vs Active TB

Gráinne Jameson[1], Isabella Batten[1], Adam H. Dyer[1], Caoimhe Geoghegan[3], Moninne Murray[3], Niamh McDonnell[3], Dearbhla M. Murphy[1], Sarah A. Connolly[1], Anne Marie McLaughlin[2,3], Cilian Ó Maoldomhnaigh[1], Laura E. Gleeson[1,3], Joseph Keane[1,2,3], Sharee A. Basdeo[1]

[1]School of Medicine, Trinity Translational Medicine Institute, St James's Hospital, Trinity College Dublin, Dublin, Ireland.
[2]National Tuberculosis Centre, Department of Respiratory Medicine, St James's Hospital, Dublin, Ireland.
[3]Respiratory Department, St James's Hospital, Dublin 8, Dublin, Ireland.

Corresponding author:
Gráinne Jameson
Trinity Translational Medicine Institute,
Trinity Centre for Health Sciences,
St. James's Hospital,
Dublin 8
GJAMESON@TCD.IE, +353 1 896 3263

Authors Contributions:
G.J. and S.A.B. conceived the study and hypotheses. G.J., I.B., A.H.D., C.G., M.M., N.M., A.M., L.E.G. and J.K. participated in data collection. J.K, L.E.G., C.O.M. and A.M. provided domain expert advice and evaluation of the project. G.J., I.B., A.H.D., D.M., S.A.C., C.O.M. and S.A.B. performed data and statistical analyses. All authors interpreted the data. G.J. and S.A.B. wrote the initial draft of the manuscript. All authors provided substantive critical reviews and approved of the submitted manuscript.

Sources of Support: This work was funded by the Health Research Board Ireland (HRB-ILP-POR-2022-033 and HRB-EIA-2019-010; awarded to S.A.B.) and The Royal City of Dublin Hospital Trust (RCDH app 185; Awarded to J.K.). The following reagent was obtained through BEI Resources, NIAID, NIH: Mycobacterium tuberculosis, Strain H37Rv, Gamma-Irradiated Whole Cells, NR-49098).

Total word count: 38033

Abstract:

Rationale:

Monocytes are central to host defence against *Mycobacterium tuberculosis* (Mtb), yet their functional and metabolic profiles during latent TB infection (TBI) and active TB disease (TBD) remain poorly defined. Immunometabolic dysfunction may underlie ineffective responses in TB, but cell-specific mechanisms are unclear.

Objectives:

To compare the phenotypic, functional, and metabolic profiles of circulating monocytes from individuals with TBI, TBD, and healthy controls (HC), and assess the impact of treatment.

Measurements:

Peripheral blood monocytes were profiled using high-dimensional flow cytometry, Luminex cytokine/chemokine assays, and SCENITH™, a flow-based metabolic assay. Unstimulated and Mtb-stimulated monocytes from treatment-naïve and treated individuals were analysed.

Main Results:

Monocytes from TBI and TBD showed distinct phenotypes from HC, marked by elevated CD14 and CD45RA. HLA-DR was reduced in TBI versus HC and further decreased in TBD. TNF receptors were downregulated in TBI but unchanged in TBD. Baseline cytokine and chemokine profiles in TBI and TBD were similar (yet distinct from HC), but Mtb stimulation elicited a stronger cytokine response in TBI. Metabolically, TBI and TBD monocytes exhibited increased glycolysis and reduced mitochondrial dependence versus HC. Treatment partially restored mitochondrial function. Upon Mtb challenge, TBI monocytes had higher glycolytic capacity than TBD.

Conclusions:

Monocyte metabolic plasticity and cytokine production distinguish latent from active TB and are partially reversible with treatment. Circulating monocyte metabolism reflects TB immune status and may serve as a biomarker or therapeutic target. Reprogrammed glycolytic profiles in TBI contrast with impaired adaptability in TBD, suggesting dysfunctional myeloid activation during disease.

Number of words: 246

Key words: Mycobacterium tuberculosis, Mitochondria, Innate Immunity, monocyte

Introduction

Tuberculosis (TB) is the leading cause of death by an infectious agent, with an estimated 1.25 million deaths and 10.8 million cases in 2023 (1). While most individuals infected with *Mycobacterium tuberculosis* (Mtb) do not progress to active disease, those with latent TB infection (TBI) carry approximately twice the risk of developing tuberculosis disease (TBD compared with uninfected individuals), yet also demonstrate a 79% lower risk of progressive disease following reinfection (2). Understanding the immunological mechanisms that confer protection in TBI or promote progression to TBD is a central question in TB research.

Monocytes are short-lived, circulating myeloid cells that play a critical role in the peripheral immune response to infection. They contribute to antimicrobial defence through phagocytosis, cytokine production, and antigen presentation (3–7). In TB, monocytes are recruited from the circulation to the lungs, the primary site of infection, where they can differentiate into alveolar macrophages (AMs) (8–12). The AM niche almost exclusively harbours early Mtb infection and acts as the first line of defence (13,14).

Cellular metabolism has emerged as a key regulator of myeloid function. Glycolysis, in particular, drives effective antimicrobial activity in both human AM and monocyte-derived macrophages responding to Mtb (15–18). Similar metabolic reprogramming occurs in healthy monocytes upon infection (19). In contrast, monocytes from individuals with TBD exhibit impaired ex vivo metabolic function, characterised by reduced glycolysis and oxidative phosphorylation compared with healthy controls (20). These deficits are partially reversible with TB treatment, suggesting that Mtb infection directly alters monocyte bioenergetics and function.

63 Together, these findings highlight the importance of immunometabolism in shaping host responses
64 to TB and support ongoing efforts to develop host-directed therapies. However, how monocyte
65 metabolism and function differ between stages of TB, particularly between TBI and TBD, remains
66 incompletely understood. In this study, we aimed to characterise the phenotypic, functional, and
67 metabolic profiles of circulating monocytes from individuals across the TB spectrum. We used
68 SCENITH™, a single-cell metabolic profiling assay, to uncover immune and bioenergetic features
69 that may distinguish infection from disease(21) (Figure 1).

70 Methods

71

72 *Human Participants*

73 All peripheral blood patient samples were collected in the out-patient department of St James's
74 Hospital Dublin when patients were attending routine appointments (Table 1). Written informed
75 consent was obtained prior to collection. Exclusion criteria included age under 18 years, inability
76 to provide written informed consent, multi-drug-resistant tuberculosis, or a known (or ensuing)
77 diagnosis of malignancy, HIV or any other infection. Individuals with TBI were selected based on
78 a positive QuantiFERON-TB Gold Plus IGRA test with absence of any clinical symptoms of TB
79 disease and were subdivided into those pre-treatment (TBI/-; n=6) and those on-treatment (TBI/+;
80 n=4). Individuals clinically diagnosed of TBD were grouped into intensive (TBD/I, <2 months
81 treatment of 3-4 drugs; n=4) and continuation (TBD/C, >2 months reduced to 1-2 drugs; n=4)
82 treatment phases. Peripheral blood samples were also obtained from healthy controls who have
83 all received BCG vaccination previously.

84

85 *PBMC and Monocyte Isolations*

86 PBMC were isolated from peripheral blood samples by density centrifugation over Lymphoprep
87 (StemCell Technologies). Monocytes were separated by hyperosmotic density gradient
88 centrifugation by layering PBMC on top of a fresh hyperosmotic Percoll solution (48.5% Percoll,
89 41.5% sterile H2O, 0.16 M NaCl) and centrifuged for 15 minutes at 580*g*. The interphase layer
90 was isolated, and cells were washed with cold PBS and resuspended at a concentration of 1 ×
91 10^6 cells/mL. Cells were plastic adhered for 1hr in serum-free medium and washed twice with PBS
92 to remove any non-adherent cells.

93

94 Irradiated H37Rv (iH37Rv; gifted by BEI Resources) stocks were thawed, sonicated for 15 mins
95 and syringed three times through a 25G needle break up clumps. iH37Rv was centrifuged at 30
96 xg for 5 mins to pellet any further clumps. Supernatant was aspirated and the concentration of
97 iH37Rv was calculated using Pierce™ BCA Protein Assay with Albumin protein as a control
98 (Thermo Scientific™). Cells were stimulated with 10 µg/mL of iH37Rv overnight for 18hours. Cells
99 were left unstimulated as a control.

100

101 *Cytokine and Chemokine Analyses*

102 A Human Luminex Discovery Kit (Cat LXSAHM-25) was designed to assess the following analytes
103 in monocyte supernatants: CCL1/I-309/TCA-3 (BR15), CCL2/JE/MCP-1 (BR25), CCL3/MIP-1
104 alpha (BR35), CCL4/MIP-1 beta (BR37), CXCL1/GRO alpha/KC/CINC-1 (BR77), CXCL2/GRO
105 beta/MIP-2/CINC-3 (BR27), CXCL9/MIG (BR52), CXCL10/IP-10/CRG-2 (BR67), G-CSF (BR54),
106 GM-CSF (BR46), Granzyme B (BR57), IFN-alpha (BR63), IFN-beta (BR21), IFN-gamma (BR29),
107 IL-1 alpha/IL-1F1 (BR38), IL-1 beta/IL-1F2 (BR28), IL-1ra/IL-1F3 (BR30), IL-6 (BR13), IL-
108 8/CXCL8 (BR18), IL-10 (BR22), IL-12 p70 (BR56), IL-17/IL-17A (BR42), IL-18/IL-1F4 (BR78), IL-
109 23 (BR76), TNF-alpha (BR12). The assay was carried out as per manufacturers protocol and

110 analysed on Luminex MAGPIX System. Unstimulated and Mtb-stimulated cells from each donor
111 were analyzed concurrently on the same plate, thereby eliminating potential inter-assay variability
112 and ensuring the accurate calculation of fold-change values. Analyte concentrations were
113 determined based on standards supplied in the kit, with a 5 parameter logistic regression (5-PL)
114 curve used on xPONENT(TM) software.
115

116 *Flow cytometry*

117 For phenotypical analyses PBMC were resuspended in PBS (Gibco) and stained immediately.
118 Anti-CD86 BV421 (1:100, IT2.2), anti-CD45RA BV711 (1:100, HI100), anti-CD40 APCCy7 (1:100,
119 5C3), anti-HLADR APC (1:100, L243), anti-CD14 AlexaFlour 488 (1:100, HCD14), anti-CD16
120 PerCpCy5.5 (1:100, 3G8), anti-CD80 PeCy7 (1:100, 2D10), anti-TNFRI PE (1:50, W15099A), and
121 anti-TNFRII PeDazzle594 (1:100, 3G7A02) were purchased from BioLegend and added to the
122 cells for 10 mins at RT. Cells were washed, fixed and acquired or stored at 4°C until acquisition.
123

124 Cultured PBMC were resuspended in 100 µl of FcR block (1µl/test; Miltenyi Biotec) and
125 ZombieNIR stain (BioLegend) in 1X PBS (Gibco). Cells were then surface stained with anti-CD14
126 and permeabilized with Foxp3 staining kit (eBioscience) according to the manufacturer's
127 instructions. Cells were incubated for 30 mins at 4°C with anti-puromycin (1:100, 2A4; BioLegend).
128 Cells were acquired on a FACS Canto (BD Biosciences), BD Fortessa, (BD Biosciences) or an
129 Amnis CellStream (Luminex Corporation, Austin, TX, USA). All data analysis was performed using
130 FlowJo software (BD Biosciences).
131

132 *SCENITH (Single Cell mEtabolism by profiling Translation inHibition)*

133 This protocol uses puromycin as a surrogate for protein synthesis, as it becomes incorporated into
134 newly formed proteins. Since protein synthesis represents around 50% of total cellular metabolic

135 activity, measuring puromycin incorporation provides a robust indicator of overall metabolic
136 activity. By measuring puromycin incorporation post-oligomycin treatment we can estimate the
137 cells dependency on mitochondrial respiration and their capacity for glycolysis. By measuring
138 puromycin incorporation post 2-Deoxy-D-Glucose (2-DG) treatment we can estimate the cells
139 dependency on glucose as a fuel and therefore their capacity for other fuels such as fatty acid and
140 amino acid oxidation. A detailed explanation of these calculations was described in our previous
141 work and in the original protocol publication (21,22). Post 18 hours of culture, SCENITH metabolic
142 function profiling was carried out on PBMCs. Cells were treated for 40 mins at 37°C, 5% CO2 with
143 DMSO Control (Co, 0.02% DMSO), 2-DG (100 mM; Sigma-Aldrich), Oligomycin (O; 1μM; Sigma-
144 Aldrich), a combination of both drugs (DGO), or with Harringtonine, which inhibits protein synthesis
145 (Sigma-Aldrich; 2 μg/ml). Puromycin (Puro; 10 μg/mL; Sigma-Aldrich) was added for the final 35
146 mins. Cells were washed in PBS and flow cytometry staining was carried out. The following
147 calculations were used:
148
149 Co = GeoMFI of anti-Puro-Fluorochrome upon DMSO Control treatment.
150 DG = GeoMFI of anti-Puro-Fluorochrome upon 2-Deoxy-D-Glucose treatment.
151 O = GeoMFI of anti-Puro-Fluorochrome upon Oligomycin A treatment.
152 DGO = GeoMFI of anti-Puro-Fluorochrome upon DG+O treatment.
153
154 Mitochondrial Dependence (MD)=100(Co-O)/(Co-DGO)
155 Glycolytic Capacity (GC)= 100-100(Co-O)/(Co-DGO)
156 Fatty Acid and Amino Acid Oxidation Capacity (FAOC)= 100-(100(Co-DG)/(Co-DGO)
157 Glucose Dependence (GD)= 100(Co-DG)/(Co-DGO)

158 Therefore, GC is the inverse data of MD (i.e. GC= 100- MD) and FAOC is the inverse data of GD
159 (i.e. FAOC= 100-GD). Patient samples with sufficient cell numbers underwent metabolic profiling.
160 No data was omitted.
161

162 *Statistics*

163 Statistical analysis was performed using GraphPad Prism version 10. The statistical test used is
164 indicated in each figure legend. A P-value of <0.05 was considered significant.
165

166 *Study Approval*

167 Our study protocol was approved by the Joint Research Ethics Committee of St. James's and
168 Tallaght Hospitals and by Trinity College Dublin. Written informed consent was received from
169 participants prior to inclusion in the study.
170

171 *Data availability*

172 Data is available directly from the corresponding author.
173
174

175 Results

176 **Altered Expression of HLA-DR, CD14, and TNFRs in Monocytes Across the TB Spectrum**

177 We next investigated whether TB infection influences monocyte frequency and phenotype across
178 the disease spectrum. No significant differences were observed in the frequencies of classical,
179 intermediate, or non-classical monocyte subsets between groups (Figure 2A–B). However,
180 phenotypic analysis revealed elevated expression intensity of CD14 and CD45RA on classical

181 monocytes from individuals with both TBI (CD14: P = 0.0039; CD45RA: P = 0.0070) and TBD
182 (CD14: P = 0.0010; CD45RA: P = 0.0007) compared with healthy controls (HC) (Figure 2C–D).
183
184 In contrast, expression of HLA-DR was significantly reduced on classical monocytes from TBI (P
185 = 0.0374) and even further reduced in TBD (P < 0.0001) compared with HC, with significantly
186 lower levels in TBD than TBI (P = 0.0068; Figure 2F). Expression of TNF receptors was decreased
187 in TBI but not TBD; both TNFRI (P = 0.0185) and TNFRII (P = 0.0414) were downregulated on
188 classical monocytes from TBI compared with HC (Figure 2G–H). Similar phenotypic changes were
189 observed in intermediate and non-classical monocyte subsets across the TB spectrum
190 (Supplemental Figure 2).
191
192 These data demonstrate that while monocyte subset frequencies remain stable, TB infection—
193 both latent and active—induces distinct phenotypic reprogramming of monocytes. Notably, the
194 progressive reduction in HLA-DR expression from TBI to TBD may reflect functional impairment,
195 with implications for antigen presentation and immune regulation during infection (23–27).
196
197 **Monocytes from TBI and TBD individuals exhibit distinct functional responses to Mtb**
198 **stimulation.**
199 To assess functional differences in monocytes across the TB spectrum, $CD14^+$ monocytes were
200 isolated from PBMC and cultured for 18 hours with or without irradiated-H37Rv (iMtb). Culture
201 supernatants were collected, and cytokine and chemokine concentrations were measured using
202 a custom Luminex multiplex bead-based immunoassay (Figure 3).
203 Unstimulated monocytes from individuals with latent TB infection (TBI, light grey) and active TB
204 disease (TBD, dark grey) displayed cytokine/chemokine profiles that were distinct from healthy
205 controls (HC, blue) (Figure 3A, C and Supplemental Figure 1A). Compared with TBD monocytes,

206 unstimulated monocytes from HC produced significantly higher levels of IL-1β (P=0.0061), GM-
207 CSF (P=0.0265), TNF-α (P=0.0237), and CXCL2 (P=0.0191), and lower levels of IL-17A
208 (P=0.0098) and CXCL9 (P=0.0353) (Figure 3A, C). Similarly, HC monocytes produced higher
209 levels of IL-1β (P=0.0053) and CXCL2 (P=0.0191), and lower levels of IL-17A (P=0.0018) than
210 monocytes from TBI individuals.
211
212 Following iMtb stimulation, monocytes from both TBI and TBD groups showed significantly
213 increased production of several cytokines and chemokines compared with HC, including IL-1α
214 (TBI: P=0.0153; TBD: P=0.0228), IL-8 (TBI: P=0.0129; TBD: P=0.0278), IL-23 (TBI: P=0.0158;
215 TBD: P=0.0400), and GM-CSF (TBI: P=0.0346; TBD: P=0.0203) (Figure 3B, D; Supplemental
216 Figure 1). Notably, despite comparable baseline cytokine production, only monocytes from TBI
217 individuals showed significantly increased levels of IL-1RA (P=0.0084), IL-17A (P=0.0171), IL-18
218 (P=0.0438), IFN-γ (P=0.0382), CXCL1 (P=0.0194), CXCL9 (P=0.0129), and CCL2 (P=0.0420)
219 compared with HC (Figure 3B, E). These findings demonstrate that while both TBI and TBD
220 monocytes respond robustly to iMtb stimulation, monocytes from individuals with TBI exhibit a
221 broader and more distinct cytokine and chemokine response compared with healthy controls. This
222 suggests that TBI monocytes may be functionally distinct from TBD monocytes, enabling a
223 heightened response to iMtb. In contrast, the blunted baseline and narrower inducible responses
224 observed in TBD may reflect monocyte dysfunction or exhaustion associated with active disease.
225
226 **Reduced mitochondrial metabolism in monocytes from TBI and TBD individuals**
227 We next compared the metabolic function of monocytes from HC, TBI, and TBD individuals using
228 the SCENITH assay, which measures puromycin incorporation as a proxy for protein synthesis, a
229 process that accounts for approximately 50% of a cell's total metabolic activity (Figure 4A). The

230 addition of metabolic inhibitors 2-DG and oligomycin enabled us to evaluate cellular dependence
231 on glycolysis and mitochondrial respiration, respectively.
232 In unstimulated conditions, monocyte metabolic activity (measured by puromycin mean
233 fluorescence intensity [MFI]) was reduced following treatment with either 2-DG or oligomycin
234 across all groups (Figure 4B), confirming sensitivity to both glycolytic and oxidative metabolic
235 pathways.
236
237 Glucose dependency, as calculated by SCENITH, was comparably high in monocytes from HC,
238 TBI, and TBD individuals (Figure 4C), indicating a shared reliance on glucose to fuel glycolysis
239 under basal conditions. In contrast, mitochondrial dependency was significantly reduced in
240 monocytes from both TBI (P = 0.01) and TBD (P = 0.0078) individuals compared with HC (Figure
241 4D), suggesting a metabolic shift away from oxidative phosphorylation. This reduction in
242 mitochondrial dependence is consistent with a compensatory increase in glycolytic capacity
243 (Figure 4E).
244
245 **TBI monocytes exhibit enhanced glycolytic response to Mtb**
246
247 Given the distinct clinical and immunological profiles of TBI and TBD, we hypothesized that
248 monocyte metabolic responses to Mtb would differ between TBI and TBD individuals. Following
249 iMtb stimulation, treatment with 2-DG significantly reduced monocyte metabolic activity in all
250 groups, confirming a strong dependence on glucose to fuel the activation-induced response
251 (Figure 4F–G).
252
253 In contrast, oligomycin treatment had no significant impact on metabolic activity post-stimulation
254 (Figure 4F), and calculated mitochondrial dependency remained low across all groups (Figure

255 4H). Notably, monocytes from TBI individuals exhibited significantly lower mitochondrial
256 dependence and higher glycolytic capacity compared with those from TBD individuals (P = 0.031),
257 indicating a more flexible metabolic profile.
258
259 Collectively, these data reveal a clear divergence in metabolic responsiveness to Mtb between
260 TBI and TBD monocytes. Monocytes from TBI individuals display enhanced glycolytic capacity
261 and reduced reliance on mitochondrial metabolism, both at baseline and in response to
262 stimulation; hallmarks of a metabolically reprogrammed, activated phenotype. In contrast, the
263 limited metabolic adaptability observed in monocytes from TBD individuals may reflect impaired
264 functional reprogramming during active disease.
265
266
267 **Treatment restores monocyte mitochondrial function toward a healthy baseline**
268 To determine whether treatment influenced monocyte phenotype or metabolic function, we further
269 stratified participants based on treatment status (Figure 5). Individuals with TBI were grouped as
270 pre-treatment (TBI/-) or on-treatment (TBI/+), and those with TBD were classified into intensive-
271 phase treatment (TBD/I, <2 months, multi-drug) or continuation-phase treatment (TBD/C, >2
272 months, reduced-drug) cohorts. CD14 expression is significantly elevated in TBI/+ (P=0.0228) and
273 TBD/I (P=0.0069) individuals (Figure 5A). CD45RA expression levels were significantly increased
274 in TBI/+ (P=0.0208), TBD/I (P=0.0310), and TBD/C (P=0.0078; Figure 5B). Of note, HLA-DR
275 expression is only significantly decreased in TBD/I (P=0.0069) and TBD/+ (P=0.0023) individuals
276 (Figure 5D), and TNFRI expression is only reduced in TBI/+ individuals (P=0.0162; Figure 5E).
277
278 Assessment of their metabolic activity revealed no differences in baseline protein synthesis
279 between these subgroups (Figure 5G). However, monocytes from TBI/- individuals showed

280 significantly reduced mitochondrial dependence compared with HC, while those from TBI/+ did
281 not (P = 0.0258; Figure 5H). Similarly, TBD/I monocytes displayed reduced mitochondrial
282 dependence compared with HC (P = 0.0198), whereas mitochondrial dependence in TBD/C
283 monocytes was not significantly different from HC (Figure 5H).
284
285 Upon iMtb stimulation, only monocytes from TBI individuals significantly increased their overall
286 metabolic activity (TBI/−: P = 0.0137; TBI/+: P = 0.0024; Figure 5I). Again, a corresponding
287 decrease in mitochondrial dependence was only observed in TBI individuals on treatment
288 (P=0.0185) and HC (P=0.0044; Figure 5J). In contrast, monocytes from TBD individuals showed
289 no significant change in either metric following iMtb stimulation, regardless of treatment phase
290 (Figure 5I-J).
291
292 These data suggest that both TBI and TBD are associated with reduced mitochondrial metabolism
293 in circulating monocytes, particularly in untreated individuals, and that both TB preventative
294 treatment (TPT) and TBD treatment may partially restore metabolic function toward a healthy
295 baseline.
296
297

298 ## Discussion

299 Our study reveals that Mtb infection induces distinct alterations in circulating monocyte phenotype,
300 function, and metabolism, that differ between individuals with TBI and TBD. Despite similar
301 monocyte subset frequencies across groups, phenotypic profiling showed that monocytes in TBI
302 individuals exhibit an upregulation of activation markers (e.g., CD14, CD45RA) alongside
303 downregulation of HLA-DR and TNF receptors, key mediators of antigen presentation and
304 inflammation. Notably, HLA-DR expression declined progressively from TBI to TBD, suggesting a

305 trajectory of monocyte dysfunction with disease progression which has been highlighted as a
306 biomarker of infection in TB, sepsis and paediatric infection (24–28). Functionally, monocytes from
307 both groups remained responsive to iMtb stimulation, but TBI monocytes exhibited a more robust
308 cytokine and metabolic response compared with TBD monocytes.
309
310 Among the analytes elevated in TBI compared with TBD and healthy controls, IL-1RA, IL-17A,
311 and CXCL9 showed the most pronounced increase, unaffected by outlier values. IL-1RA, an
312 antagonist of IL-1α/β signalling produced predominantly by monocytes and neutrophils, has been
313 proposed as a biomarker for TB spectrum stratification (29). In our study, IL-1RA was significantly
314 upregulated in monocytes from individuals with TBI, but not from those with TBD, supporting a
315 potential role for monocyte-derived IL-1RA in maintaining infection containment. However,
316 previous findings on IL-1RA expression in TB have been inconsistent, with some studies reporting
317 higher IL-1RA levels in response to TB antigens in TBD relative to TBI, and others showing the
318 opposite (30–33). Notably, these prior studies were based on whole blood or PBMC cultures,
319 making it difficult to resolve cell-specific contributions. By focusing on purified monocytes, our data
320 provide more direct evidence that monocyte-specific IL-1RA production may differentiate TBI from
321 TBD.
322
323 Similarly, we observed significant upregulation of IL-17A and CXCL9 in monocytes from TBI but
324 not TBD individuals (Figure 1E). CXCL9 acts as a critical chemoattractant for $CXCR3^{+}$ T cells,
325 facilitating the recruitment and activation of IFN-γ–producing effector T cells (34). IL-17A is a
326 potent inducer of chemokines that recruit immune cells such as T cells and neutrophils, and
327 stimulates antimicrobial peptide production from epithelial cells (35). Collectively, this monocyte
328 cytokine and chemokine profile characterized by elevated IL-1RA, IL-17A, and CXCL9 in TBI may
329 reflect an immunological environment conducive to effective containment of Mtb infection.

330

331 We hypothesize that the distinct effector cytokine and chemokine profile observed in monocytes
332 from individuals with TBI is underpinned by metabolic reprogramming that favours glycolysis over
333 mitochondrial respiration. TBI monocytes displayed enhanced glycolytic capacity and reduced
334 mitochondrial dependence both at rest and upon stimulation, consistent with an activated
335 immunometabolic phenotype (Figure 4D-E). In contrast, TBD monocytes failed to undergo this
336 shift, suggesting impaired metabolic plasticity which supports previous reports of their overall
337 diminished bioenergetics (20). Given the known link between glycolysis and effector function, this
338 metabolic rewiring is likely associated with the enhanced production of cytokines and chemokine
339 observed specifically in TBI monocytes, which may facilitate the effective immune containment of
340 Mtb. Of note, to assess differential sustained metabolic responses of monocytes to Mtb between
341 TBI and TBD individuals, cells were cultured for 18 hours with iMtb followed by the SCENITH
342 protocol. We acknowledge that future studies incorporating Seahorse Analyzer assays on freshly
343 isolated monocytes may provide further insight into the dynamic and immediate metabolic
344 changes that occur upon iMtb stimulation.

345

346 These data resonate with and extend the work of other research groups investigating host
347 metabolic responses in TB. Notably, bioenergetic dysfunction of monocytes in South African TBD
348 cohorts have been reported (20). In addition, myeloid cell metabolic rewiring governs innate
349 immune cell function in the context of BCG vaccination (36) and heterologous innate immunity to
350 Mtb elicited by adenoviral vectored COVID-19 vaccination (37). Our findings complement and
351 build upon these studies by focusing specifically on purified circulating monocytes metabolic
352 capacity and effector cytokine output across the TB spectrum.

353

354 Importantly, our findings also indicate that treatment, including TPT in TBI and multidrug regimens
355 in TBD, partially restores mitochondrial function in circulating monocytes, shifting their metabolic
356 baseline profile closer to that of healthy individuals. This suggests that monocyte metabolism is
357 dynamic and responsive to therapeutic intervention, indicating that mitochondrial dependency
358 metrics hold potential as a novel biomarker for treatment efficacy and disease resolution.
359 Moreover, these insights underscore the therapeutic potential of targeting monocyte metabolic
360 pathways to enhance host immune function in TB.
361
362 These results contribute to a growing body of evidence that immunometabolism shapes infection
363 outcomes in TB. Since circulating monocytes give rise to macrophages, including lung-resident
364 alveolar macrophages, targeting metabolic pathways in monocytes may enhance both peripheral
365 and pulmonary immune responses (38–40). Although our study focused on peripheral blood
366 monocytes, it is reasonable to hypothesize that some aspects of monocyte immunometabolic
367 reprogramming are reflected in lung-resident or recruited mononuclear phagocytes, given the
368 dynamic trafficking of monocytes from blood to tissue. However, the lung microenvironment may
369 also induce additional, tissue-specific metabolic adaptations that could modify these peripheral
370 phenotypes. Recent evidence indicates that human airway macrophages are metabolically and
371 functionally distinct from monocyte-derived macrophages in response to Mtb (41,42) and murine
372 studies highlight the metabolic heterogeneity across alveolar and interstitial lung macrophages in
373 response to Mtb (18). If future studies reveal differences between systemic and local immune
374 programming, this will underscore compartmentalized immune responses, helping to delineate
375 distinct mechanisms of immune protection or pathogenesis in TB. Importantly, such insights
376 reinforce the potential of monocyte metabolism as a promising target for host-directed therapies,
377 particularly those aimed at preventing progression from TBI to TBD by enhancing both systemic
378 and lung-localized immunity.

While our study provides novel insights into monocyte immunometabolism across the TB spectrum, several limitations should be acknowledged. First, the relatively small sample size may limit the generalizability of our findings and the statistical power to detect more subtle differences or correlations with clinical outcomes. Second, we did not establish a direct link between the observed monocyte metabolic and phenotypic changes and disease progression or treatment success, which will require longitudinal studies with larger cohorts. Third, our functional assays utilized irradiated H37Rv. This well-characterized lab strain facilitates standardization however, future studies incorporating live, virulent strains are essential to fully elucidate how pathogen variability shapes host monocyte responses. Despite these limitations, our data provide a valuable foundation for future investigations aimed at elucidating the functional benefits of this metabolic plasticity in TBI, and its impact on bacterial killing. Such studies will be essential for identifying robust biomarkers and therapeutic targets through detailed mechanistic analyses of monocyte immunometabolism in tuberculosis.

In summary, our data reveal that Mtb infection drives distinct immunometabolic changes in circulating monocytes with TBI characterised by functional responsiveness and glycolytic, pro-inflammatory profile, while TBD is marked by impaired metabolic plasticity. Furthermore, we show that TB treatment of both TBI and TBD individuals may restore monocyte mitochondrial function. These findings offer important insight into the cellular mechanisms of immune containment in TB and support the rationale for treating TBI. Moreover, they underscore the potential of monocyte metabolism as a biomarker of disease state and a tractable target for host-directed therapies. Continued research building on these insights will be crucial for advancing TB diagnosis, monitoring treatment efficacy, and developing novel interventions to improve patient outcomes.

Acknowledgements

We sincerely thank all the individuals who participated in this study. We are especially grateful to the patients for their time, generosity, and willingness to contribute to research aimed at improving the understanding and treatment of tuberculosis. Their participation made this work possible. The following reagent was obtained through BEI Resources, NIAID, NIH: Mycobacterium tuberculosis, Strain H37Rv, Gamma-Irradiated Whole Cells, NR-49098. We gratefully acknowledge the support of the Core Flow Cytometry Facility and Prof. Nollaig Bourke's research team at the Trinity Translational Medicine Institute.

413 References

414 1. Geneva WHO. *Global Tuberculosis Report 2024*.; 2024.

415 2. Andrews JR, Noubary F, Walensky RP, Cerda R, Losina E, Horsburgh CR. Risk of
416 Progression to Active Tuberculosis Following Reinfection With Mycobacterium
417 tuberculosis. *Clin Infect Dis An Off Publ Infect Dis Soc Am*. 2012;54(6):784.
418 doi:10.1093/CID/CIR951

419 3. Sampath P, Moideen K, Ranganathan UD, Bethunaickan R. Monocyte Subsets:
420 Phenotypes and Function in Tuberculosis Infection. *Front Immunol*. 2018;9:1726.
421 doi:10.3389/FIMMU.2018.01726

422 4. Wolf Y, Shemer A, Polonsky M, et al. Autonomous TNF is critical for in vivo monocyte
423 survival in steady state and inflammation. *J Exp Med*. 2017;214(4):905.
424 doi:10.1084/JEM.20160499

425 5. Netea MG, Nold-Petry CA, Nold MF, et al. Differential requirement for the activation of the
426 inflammasome for processing and release of IL-1beta in monocytes and macrophages.
427 *Blood*. 2009;113(10):2324-2335. doi:10.1182/BLOOD-2008-03-146720

428 6. Affandi AJ, Olesek K, Grabowska J, et al. CD169 Defines Activated CD14+ Monocytes
429 With Enhanced CD8+ T Cell Activation Capacity. *Front Immunol*. 2021;12:697840.
430 doi:10.3389/FIMMU.2021.697840/FULL

431 7. Guilliams M, Mildner A, Yona S. Developmental and Functional Heterogeneity of
432 Monocytes. *Immunity*. 2018;49(4):595-613. doi:10.1016/J.IMMUNI.2018.10.005

433 8. Serbina N V., Pamer EG. Monocyte emigration from bone marrow during bacterial
434 infection requires signals mediated by chemokine receptor CCR2. *Nat Immunol*.
435 2006;7(3):311-317. doi:10.1038/NI1309

436 9. McQuattie-Pimentel AC, Budinger GRS, Ballinger MN. Monocyte-derived Alveolar
437 Macrophages: The Dark Side of Lung Repair? *Am J Respir Cell Mol Biol*. 2018;58(1):5-6.

438 doi:10.1165/RCMB.2017-0328ED
439 10. Misharin A V., Morales-Nebreda L, Reyfman PA, et al. Monocyte-derived alveolar
440 macrophages drive lung fibrosis and persist in the lung over the life span. *J Exp Med*.
441 2017;214(8):2387-2404. doi:10.1084/JEM.20162152
442 11. Machiels B, Dourcy M, Xiao X, et al. A gammaherpesvirus provides protection against
443 allergic asthma by inducing the replacement of resident alveolar macrophages with
444 regulatory monocytes. *Nat Immunol*. 2017;18(12):1310-1320. doi:10.1038/NI.3857
445 12. Aegerter H, Kulikauskaite J, Crotta S, et al. Influenza-induced monocyte-derived alveolar
446 macrophages confer prolonged antibacterial protection. *Nat Immunol 2020 212*.
447 2020;21(2):145-157. doi:10.1038/s41590-019-0568-x
448 13. Srivastava S, Ernst JD, Desvignes L. Beyond macrophages: the diversity of mononuclear
449 cells in tuberculosis. *Immunol Rev*. 2014;262(1):179. doi:10.1111/IMR.12217
450 14. Cohen SB, Gern BH, Delahaye JL, et al. Alveolar Macrophages Provide an Early
451 Mycobacterium tuberculosis Niche and Initiate Dissemination. *Cell Host Microbe*.
452 2018;24(3):439-446.e4. doi:10.1016/J.CHOM.2018.08.001
453 15. Gleeson LE, Sheedy FJ, Palsson-McDermott EM, et al. Cutting Edge: Mycobacterium
454 tuberculosis Induces Aerobic Glycolysis in Human Alveolar Macrophages That Is
455 Required for Control of Intracellular Bacillary Replication . *J Immunol*. 2016;196(6):2444-
456 2449. doi:10.4049/jimmunol.1501612
457 16. Mendonca LE, Pernet E, Khan N, et al. Human alveolar macrophage metabolism is
458 compromised during Mycobacterium tuberculosis infection. *Front Immunol*. 2023;13.
459 doi:10.3389/FIMMU.2022.1044592/PDF
460 17. Cumming BM, Addicott KW, Adamson JH, Steyn AJC. Mycobacterium tuberculosis
461 induces decelerated bioenergetic metabolism in human macrophages. *Elife*. 2018;7.
462 doi:10.7554/eLife.39169

463 18. Huang L, Nazarova E V., Tan S, Liu Y, Russell DG. Growth of Mycobacterium
464 tuberculosis in vivo segregates with host macrophage metabolism and ontogeny. *J Exp*
465 *Med*. 2018;215(4):1135-1152. doi:10.1084/JEM.20172020,
466 19. Lachmandas E, Beigier-Bompadre M, Cheng SC, et al. Rewiring cellular metabolism via
467 the AKT/mTOR pathway contributes to host defence against Mycobacterium tuberculosis
468 in human and murine cells. *Eur J Immunol*. 2016;46(11):2574-2586.
469 doi:10.1002/EJI.201546259;PAGE:STRING:ARTICLE/CHAPTER
470 20. Cumming BM, Addicott KW, Maruri F, et al. Longitudinal mitochondrial bioenergetic
471 signatures of blood monocytes and lymphocytes improve during treatment of drug-
472 susceptible pulmonary tuberculosis patients Monocyte/lymphocyte bioenergetic
473 signatures post-TB treatment. *Front Immunol*. 2024;15:1465448.
474 doi:10.3389/fimmu.2024.1465448
475 21. Argüello RJ, Combes AJ, Char R, et al. SCENITH: A Flow Cytometry-Based Method to
476 Functionally Profile Energy Metabolism with Single-Cell Resolution. *Cell Metab*.
477 2020;32(6):1063-1075.e7. doi:10.1016/J.CMET.2020.11.007
478 22. Jameson G, Walsh A, Woods R, et al. Human tissue-resident NK cells in the lung have a
479 higher glycolytic capacity than non-tissue-resident NK cells in the lung and blood. *Proc*
480 *Natl Acad Sci*. 2024;121(42):2412489121. doi:10.1073/PNAS.2412489121
481 23. Ansari MA, Das S, Rai G, et al. Low monocytic HLA-DR expression in critically ill patients
482 of sepsis: An indicator for antimicrobial and/or immunomodulatory intervention. *Transpl*
483 *Immunol*. 2023;81. doi:10.1016/j.trim.2023.101942
484 24. Quadrini KJ, Patti-Diaz L, Maghsoudlou J, Cuomo J, Hedrick MN, McCloskey TW. A flow
485 cytometric assay for HLA-DR expression on monocytes validated as a biomarker for
486 enrollment in sepsis clinical trials. *Cytom Part B - Clin Cytom*. 2021;100(1):103-114.
487 doi:10.1002/CYTO.B.21987;CTYPE:STRING:JOURNAL

488 25. Fumeaux T, Pugin J. Role of interleukin-10 in the intracellular sequestration of human
489 leukocyte antigen-DR in monocytes during septic shock. *Am J Respir Crit Care Med*.
490 2002;166(11):1475-1482. doi:10.1164/RCCM.200203-
491 217OC;JOURNAL:JOURNAL:AJRCCM;WGROUP:STRING:DEFAULT
492 26. Brandes-Leibovitz R, Riza A, Yankovitz G, et al. Sepsis pathogenesis and outcome are
493 shaped by the balance between the transcriptional states of systemic inflammation and
494 antimicrobial response. *Cell Reports Med*. 2024;5(11). doi:10.1016/j.xcrm.2024.101829
495 27. Leventogiannis K, Kyriazopoulou E, Antonakos N, et al. Toward personalized
496 immunotherapy in sepsis: The PROVIDE randomized clinical trial. *Cell Reports Med*.
497 2022;3(11). doi:10.1016/j.xcrm.2022.100817
498 28. Juskewitch JE, Abraham RS, League SC, et al. Monocyte HLA-DR expression and
499 neutrophil CD64 expression as biomarkers of infection in critically ill neonates and infants.
500 *Pediatr Res*. 2015;78(6):683-690.
501 doi:10.1038/PR.2015.164;SUBJMETA=2421,250,255,53,631,692;KWRD=DIAGNOSTIC+
502 MARKERS,INFECTIOUS+DISEASES
503 29. Chegou NN, Heyckendorf J, Walzl G, Lange C, Ruhwald M. Beyond the IFN-γ horizon:
504 Biomarkers for immunodiagnosis of infection with Mycobacterium tuberculosis. *Eur Respir*
505 *J*. 2014;43(5):1472-1486. doi:10.1183/09031936.00151413,
506 30. Wergeland I, Assmus J, Dyrhol-Riise AM. Cytokine Patterns in Tuberculosis Infection; IL-
507 1ra, IL-2 and IP-10 Differentiate Borderline QuantiFERON-TB Samples from Uninfected
508 Controls. *PLoS One*. 2016;11(9):e0163848. doi:10.1371/JOURNAL.PONE.0163848
509 31. Sanchez C, Jaramillo-Valverde L, Capristano S, et al. Antigen-Induced IL-1RA Production
510 Discriminates Active and Latent Tuberculosis Infection. *Microorganisms*. 2023;11(6).
511 doi:10.3390/MICROORGANISMS11061385,
512 32. Akashi S, Suzukawa M, Takeda K, et al. IL-1RA in the supernatant of QuantiFERON-TB

513 Gold In-Tube and QuantiFERON-TB Gold Plus is useful for discriminating active
514 tuberculosis from latent infection. *J Infect Chemother*. 2021;27(4):617-624.
515 doi:10.1016/J.JIAC.2020.11.023
516 33. Llibre A, Smith N, Rouilly V, et al. Tuberculosis alters immune-metabolic pathways
517 resulting in perturbed IL-1 responses. *Front Immunol*. 2022;13:897193.
518 doi:10.3389/FIMMU.2022.897193/BIBTEX
519 34. Lugassy J, Abdala-Saleh N, Jarrous G, et al. Development of DPP-4-resistant CXCL9-Fc
520 and CXCL10-Fc chemokines for effective cancer immunotherapy. *Proc Natl Acad Sci U S*
521 *A*. 2025;122(16):e2501791122.
522 doi:10.1073/PNAS.2501791122/SUPPL_FILE/PNAS.2501791122.SAPP.PDF
523 35. Lindén A, Laan M, Anderson GP. Neutrophils, interleukin-17A and lung disease. *Eur*
524 *Respir J*. 2005;25(1):159-172. doi:10.1183/09031936.04.00032904
525 36. Arts RJW, Carvalho A, La Rocca C, et al. Immunometabolic Pathways in BCG-Induced
526 Trained Immunity. *Cell Rep*. 2016;17(10):2562-2571. doi:10.1016/j.celrep.2016.11.011
527 37. Murphy DM, Cox DJ, Connolly SA, et al. Trained immunity is induced in humans after
528 immunization with an adenoviral vector COVID-19 vaccine. *J Clin Invest*. 2023;133(2).
529 doi:10.1172/JCI162581
530 38. Suzuki H, Hisamatsu T, Chiba S, et al. Glycolytic pathway affects differentiation of human
531 monocytes to regulatory macrophages. *Immunol Lett*. 2016;176:18-27.
532 doi:10.1016/J.IMLET.2016.05.009
533 39. Russell DG, Simwela N V., Mattila JT, Flynn J, Mwandumba HC, Pisu D. How
534 macrophage heterogeneity affects tuberculosis disease and therapy. *Nat Rev Immunol*.
535 Published online January 7, 2025. doi:10.1038/S41577-024-01124-3
536 40. Niec RE, Rudensky AY, Fuchs E. Inflammatory adaptation in barrier tissues. *Cell*.
537 2021;184(13):3361-3375. doi:10.1016/J.CELL.2021.05.036

538 41. Mendonca LE, Pernet E, Khan N, et al. Human alveolar macrophage metabolism is
539 compromised during Mycobacterium tuberculosis infection. *Front Immunol*. 2023;13.
540 doi:10.3389/fimmu.2022.1044592
541 42. Cox DJ, Connolly SA, Maoldomhnaigh CÓ, et al. Human airway macrophages are
542 metabolically reprogrammed by IFN-γ resulting in glycolysis dependent functional
543 plasticity. *Elife*. 2024;13. doi:10.7554/ELIFE.98449.3
544
545

546 Figure Legends

547 **Figure 1. Schematic of study design for analysis of monocyte phenotype, function and**
548 **metabolism.** Peripheral blood samples were collected from healthy controls (HC), people with
549 TBI and people with TBD and PBMC were isolated by density centrifugation. Isolated PBMCs
550 were stained for flow cytometry analysis of monocyte expression levels of CD14, CD45RA,
551 CD40, HLA-DR, TNFRI and TNFRII. Monocytes were isolated from PBMCs using density
552 centrifugation with a Percoll gradient followed by 1hr plastic adherence. Purified monocytes were
553 then cultured, with or without irradiated-H37Rv (iMtb), for 18 hours. The supernatants were
554 harvested and analysed for cytokine and chemokine concentrations. PBMC were plated for 24
555 hours with or without iMtb. Puromycin and metabolic inhibitors (2-DG and oligomycin) were
556 added for 40 mins and then the cells were stained for flow cytometry analysis. Cells were
557 washed and stained with fluorochrome-conjugated antibodies against CD14 and puromycin and
558 analyzed by flow cytometry. Puromycin MFI levels measure overall protein synthesis and act as
559 a surrogate for metabolic activity. Created in https://BioRender.com.

560

561 **Figure 2. Distinct phenotype in monocytes from individuals with TBI.** PBMC were isolated
562 from peripheral blood and stained for flow cytometry analysis. **A-B)** Representative flow plot of
563 gating strategy (A) and bar chart of monocyte subset frequencies as percentage of total
564 monocytes (B). **C-H)** Expression levels of CD14 (C), CD45RA (D) and CD40 (E) and HLA-DR
565 (F), TNFRI (G) and TNFRII (H) on classical monocytes across HC, TBI and TBD. P values
566 generated using Two-Way ANOVA with Tukey's multiple comparison test (B) and Kruskal Wallis
567 test with Dunn's multiple comparison (C-H), *P<0.05, **P<0.01, ***P<0.001, ****P<0.0001 or
568 Mann Whitney test, ##, P<0.01 (F).

569

570 **Figure 3. Monocytes from TBI individuals' distinct cytokine and chemokine production in**
571 **response to Mtb.** Monocytes were isolated from PBMC and cultured for 18 hours with and
572 without irradiated H37Rv (iMtb). [Healthy controls (HC, n=5)), latent (TBI, n=8) and Active (TBD,
573 n=5) TB patients]. **A-B)** Mean levels of cytokine and chemokine concentrations (pg/mL) in
574 supernatants collected from unstimulated (A) and iH37Rv (iMtb) stimulated (B) monocyte
575 cultures [HC (blue), TBI (light grey) and TBD (dark grey]. **C)** Differential concentration of
576 cytokines and chemokines in unstimulated monocytes. **D-E)** Analytes that are significantly
577 increased in both TBI and TBD individual's monocytes (D) and in only TBI individual's
578 monocytes (E). P values calculated using Kruskal Wallis test and Dunn's multiple comparison
579 test.

580

581 **Figure 4. Monocyte metabolic response to Mtb is distinct in TBI.** PBMC were isolated from
582 peripheral blood and cultured with or without irradiated H37Rv (iMtb) 10ug/mL for 18 hr. Post-
583 18hr PBMC cultures were treated with DMSO control or metabolic inhibitors 2-deoxyglucose
584 (2DG), oligomycin (Oligo), or combinations of both, or harringtonine, which inhibits protein
585 synthesis and acts as a negative control for this assay. Puromycin was then added, and cells
586 were cultured for 40 min. Cells were washed and stained with fluorochrome-conjugated
587 antibodies against CD14 and puromycin and analyzed by flow cytometry. Puromycin MFI levels
588 measure overall protein synthesis and act as a surrogate for metabolic activity. **A)**
589 Representative flow cytometry gating strategy showing the analyses of monocytes and their
590 puromycin staining across metabolic treatments. **B)** Puromycin MFI values measuring overall
591 metabolic activity in unstimulated monocytes across untreated (-, DMSO control), 2DG, and

592 oligomycin treatments, from HC (n=10) and people with TBI (n=10) and TBD (n=8). **C-E)**
593 Unstimulated monocytes percentage glucose (C) and mitochondrial (D) dependence and
594 glycolytic capacity (E) across all cohorts. **F)** Puromycin MFI values measuring overall metabolic
595 activity in iMtb-stimulated monocytes across untreated, 2DG, and oligomycin treatments from
596 HC (n=6) and people with TBI (n=8) and TBD (n=6). **G-I)** iMtb-stimulated monocytes percentage
597 glucose (G) and mitochondrial (H) dependence and glycolytic capacity (I) across all cohorts. P
598 values generated using Two-Way ANOVA with Dunnett's (B, F), Kruskal Wallis test with Dunn's
599 multiple comparison (D, E) and Mann Whitney test (H).

600

601 **Figure 5. Treatment impact on monocyte phenotype and function.**

602 PBMC were isolated from peripheral blood and analysed by flow cytometry or cultured with or
603 without irradiated H37Rv (iMtb) 10ug/mL for 18 hr. **A-F)** Expression levels of CD14 (A), CD45RA
604 (B) and CD40 (C) and HLA-DR (D), TNFRI (E) and TNFRII (F) on classical monocytes ex vivo.
605 Post-18hr PBMC cultures were treated with DMSO control or metabolic inhibitors 2-deoxyglucose
606 (2DG), oligomycin (Oligo), or combinations of both, or harringtonine, which inhibits protein
607 synthesis and acts as a negative control for this assay. Puromycin was then added, and cells were
608 cultured for 40 min. Cells were washed and stained with fluorochrome-conjugated antibodies
609 against CD14 and puromycin and analyzed by flow cytometry. Puromycin MFI levels measure
610 overall protein synthesis and act as a surrogate for metabolic activity. **G)** Puromycin MFI values
611 measuring overall metabolic activity in unstimulated, DMSO control-treated, monocytes in HC
612 (n=10), TBI pre-treatment (TBI/-, n=6) and TBI on-treatment (TBI/+, n=4) and TBD in the intensive
613 (TBD/I, n=4)) and continuation (TBD/C, n=4) treatment phase. **H)** Percent mitochondrial
614 dependence in unstimulated monocytes. **I)** Puromycin MFI values measuring overall change in

615 metabolic activity from unstimulated (white) to iH37Rv-stimulated (blue) monocytes. **J)** Change in
616 percentage mitochondrial dependence in iH37Rv (iMtb)-stimulated monocytes. P values
617 generated using Two-Way ANOVA with Sidak's multiple comparison test.
618

619 **Supplemental Figure 1. Raw concentration values for monocyte cytokine and chemokine**
620 **production.**

621 Monocytes were isolated from PBMC and cultured for 18 hrs with and without irradiated H37Rv
622 (iMtb). **A-B)** Concentration of cytokines and chemokines (pg/mL) in supernatants collected from
623 unstimulated (A) and iMtb-stimulated (B) monocyte cultures. P values generated using 2 Way
624 ANOVA with Tukey's multiple comparison test.

625

626 **Supplemental Figure 2. TB infection alters intermediate and non-classical monocyte**
627 **phenotype.**

628 PBMC were isolated from peripheral blood and stained for flow cytometry analysis. **A-B)** MFI
629 values for CD14, HLA-DR, CD45RA, CD40, TNFRI, and TNFRII expression on intermediate (A)
630 and non-classical (B) monocytes across HC, TBI and TBD. P values generated using Two-Way
631 ANOVA with Tukey's multiple comparison test.

632
633
634
635
636

637

638

639 Tables

640

	HC	TBI	TBD
Age	38+/-15	44.90+/-12.81	41.25+/-18.43
Gender	F (9) M (1)	M (11) F (10)	M (10) F (6)
Ethnicity (self-reported)	European (9) African (1)	Asian (10), European (4), African (2), Indian (2), Not reported (3)	Asian (4), European (5), African (7),
Site of Mtb infection	N/A	N/A	Pulmonary (6), Extra-pulmonary (7), Both (2)

641 Table 1: Patient information. HC=Healthy Controls, TBI= Tuberculosis Infection, TBD=

642 tuberculosis disease, F= female, M=male.

643

644

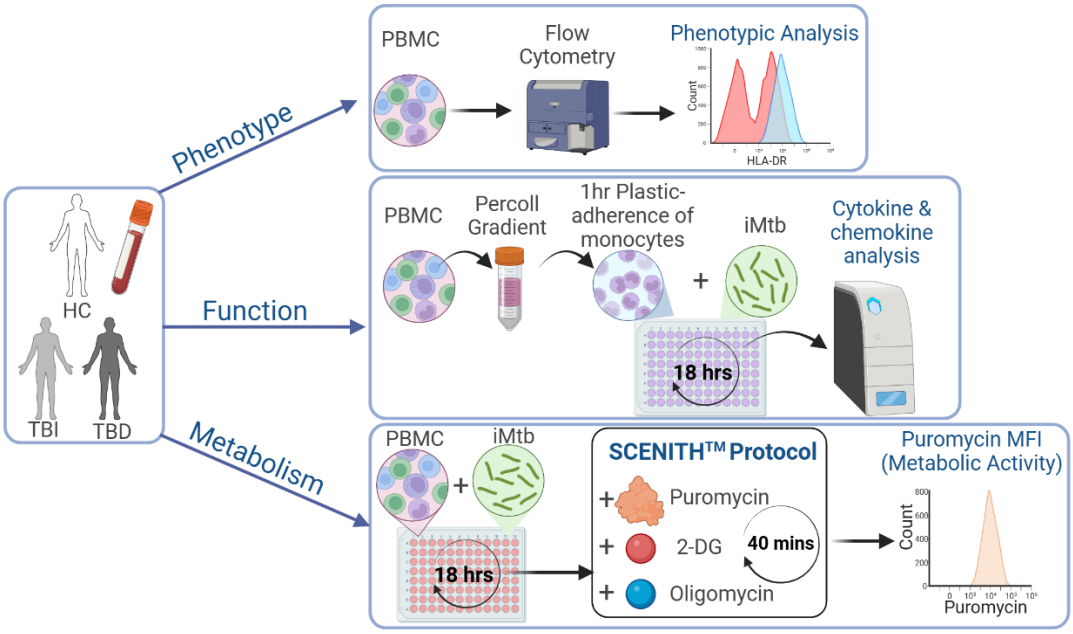
Phenotype
Function
Metabolism
HC
TBI
TBD
PBMC
Flow Cytometry
Phenotypic Analysis
Count
HLA-DR
PBMC
Percoll Gradient
1hr Plastic-adherence of monocytes
iMtb
Cytokine & chemokine analysis
18 hrs
PBMC
iMtb
18 hrs
SCENITH™ Protocol
Puromycin
2-DG
40 mins
Oligomycin
Puromycin MFI (Metabolic Activity)
Count
Puromycin

Figure 1

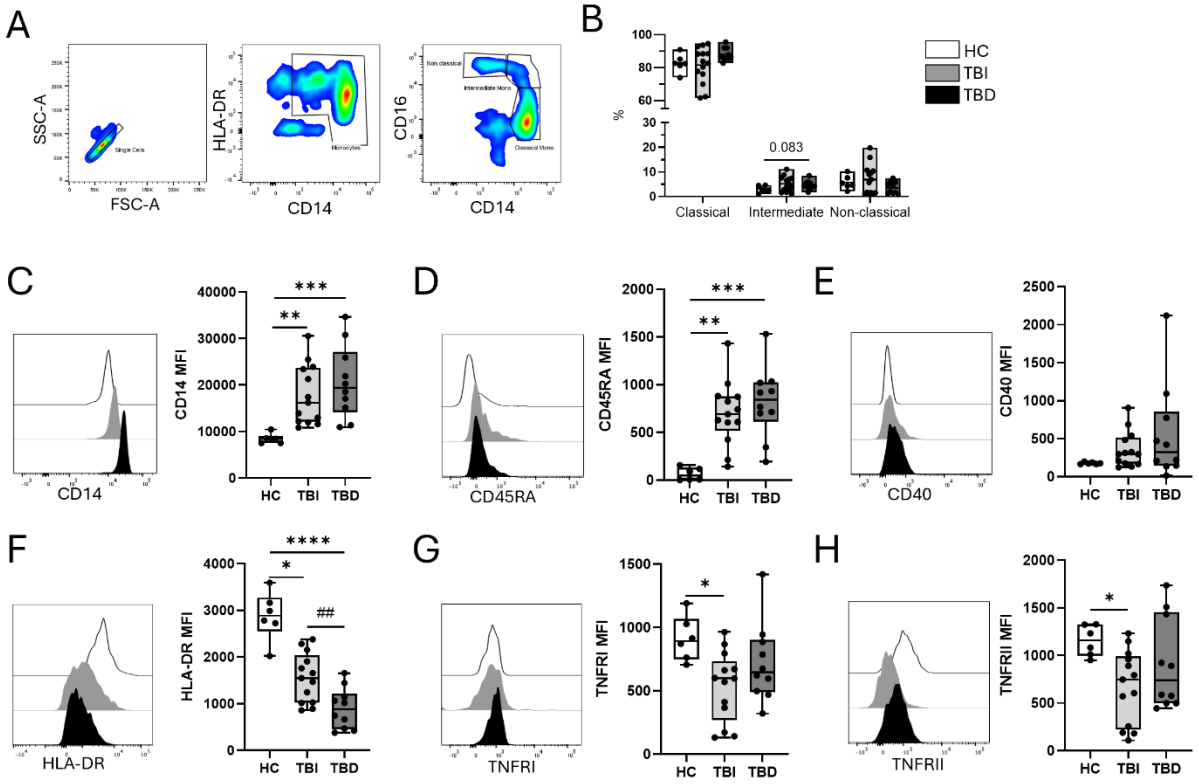
A
SSC-A
FSC-A
HLA-DR
CD14
CD16
CD14
B
HC
TBI
TBD
%
0.083
Classical
Intermediate
Non-classical
C
CD14
CD14 MFI
D
CD45RA
CD45RA MFI
E
CD40
CD40 MFI
F
HLA-DR
HLA-DR MFI
G
TNFRI
TNFRI MFI
H
TNFRII
TNFRII MFI
HC
TBI
TBD

Figure 2

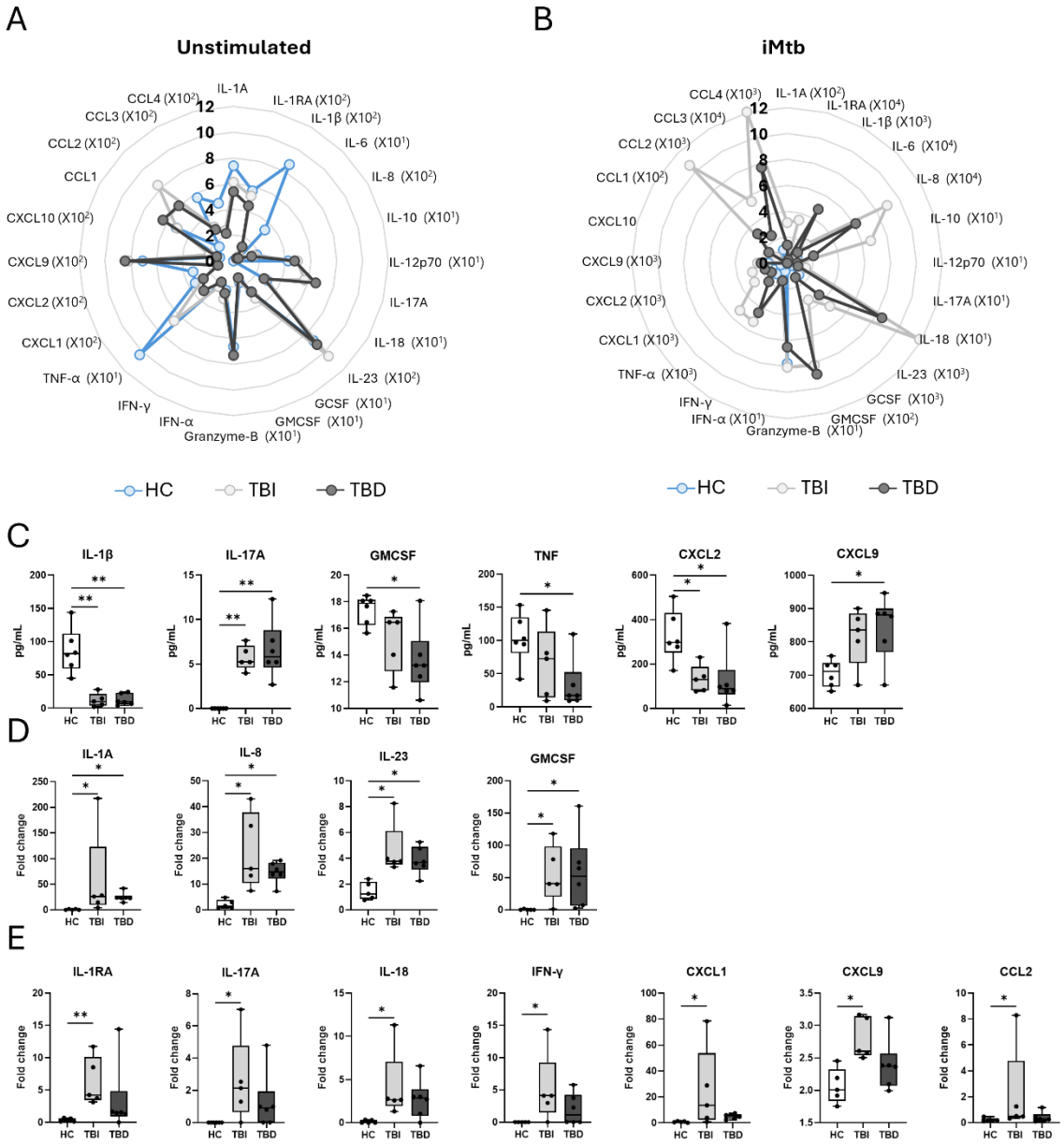
A
Unstimulated
IL-1A
IL-1RA (X10²)
IL-1β (X10²)
IL-6 (X10¹)
IL-8 (X10²)
IL-10 (X10¹)
IL-12p70 (X10¹)
IL-17A
IL-18 (X10¹)
IL-23 (X10²)
GCSF (X10¹)
GMCSF (X10¹)
Granzyme-B (X10¹)
IFN-α
IFN-γ
TNF-α (X10¹)
CXCL1 (X10²)
CXCL2 (X10²)
CXCL9 (X10²)
CXCL10 (X10²)
CCL1
CCL2 (X10²)
CCL3 (X10²)
CCL4 (X10²)
HC
TBI
TBD
B
iMtb
CCL4 (X10³)
IL-1A (X10²)
IL-1RA (X10⁴)
IL-1β (X10³)
IL-6 (X10⁴)
IL-8 (X10⁴)
IL-10 (X10¹)
IL-12p70 (X10¹)
IL-17A (X10¹)
IL-18 (X10¹)
IL-23 (X10³)
GCSF (X10³)
GMCSF (X10²)
Granzyme-B (X10¹)
IFN-α (X10¹)
IFN-γ
TNF-α (X10³)
CXCL1 (X10³)
CXCL2 (X10³)
CXCL9 (X10³)
CXCL10
CCL1 (X10²)
CCL2 (X10³)
CCL3 (X10⁴)
HC
TBI
TBD
C
IL-1β
IL-17A
GMCSF
TNF
CXCL2
CXCL9
pg/mL
HC
TBI
TBD
D
IL-1A
IL-8
IL-23
GMCSF
Fold change
HC
TBI
TBD
E
IL-1RA
IL-17A
IL-18
IFN-γ
CXCL1
CXCL9
CCL2
Fold change
HC
TBI
TBD

Figure 3

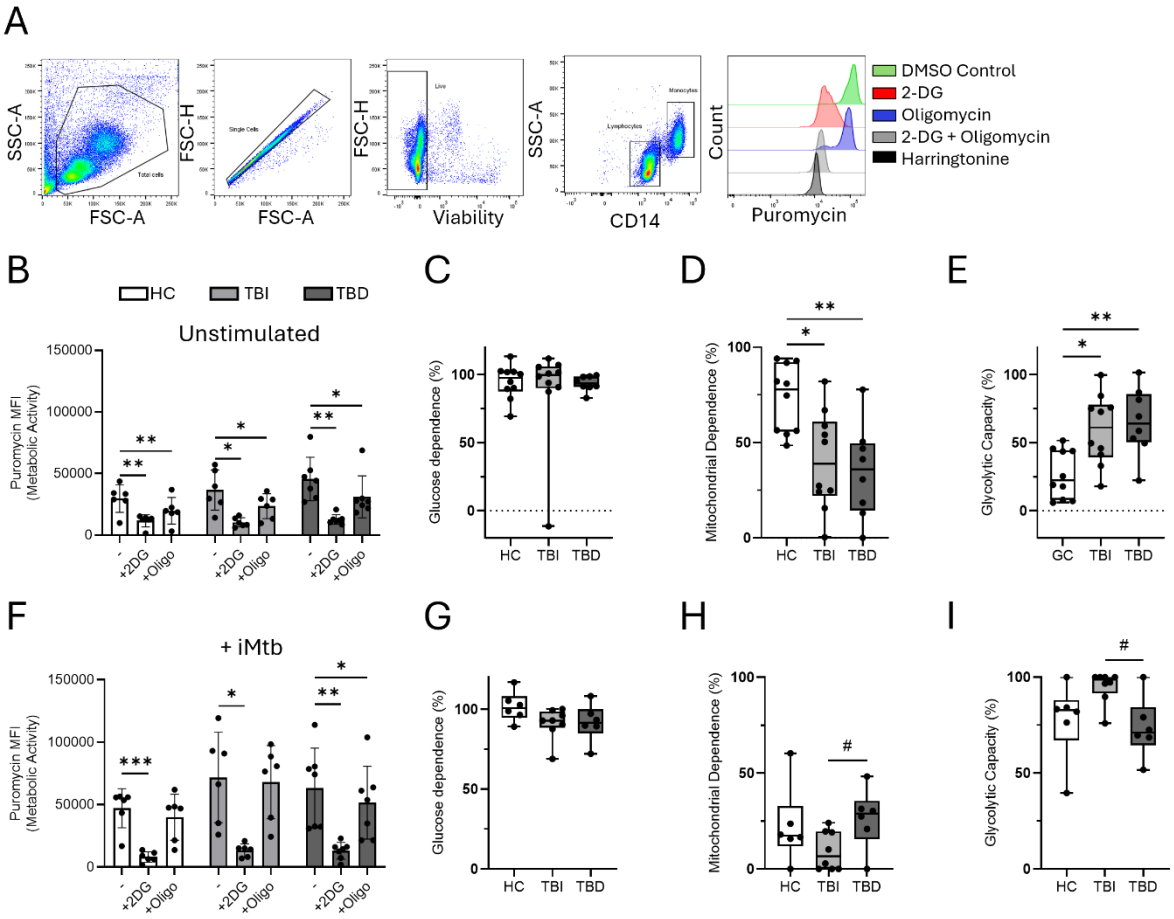
A
SSC-A
FSC-A
FSC-H
FSC-A
FSC-H
Viability
SSC-A
CD14
Count
Puromycin
DMSO Control
2-DG
Oligomycin
2-DG + Oligomycin
Harringtonine
B
HC
TBI
TBD
Unstimulated
Puromycin MFI (Metabolic Activity)
150000
100000
50000
0
-
+2DG
+Oligo
C
Glucose dependence (%)
HC
TBI
TBD
D
Mitochondrial Dependence (%)
E
Glycolytic Capacity (%)
GC
F
+ iMtb
G
H
I

Figure 4

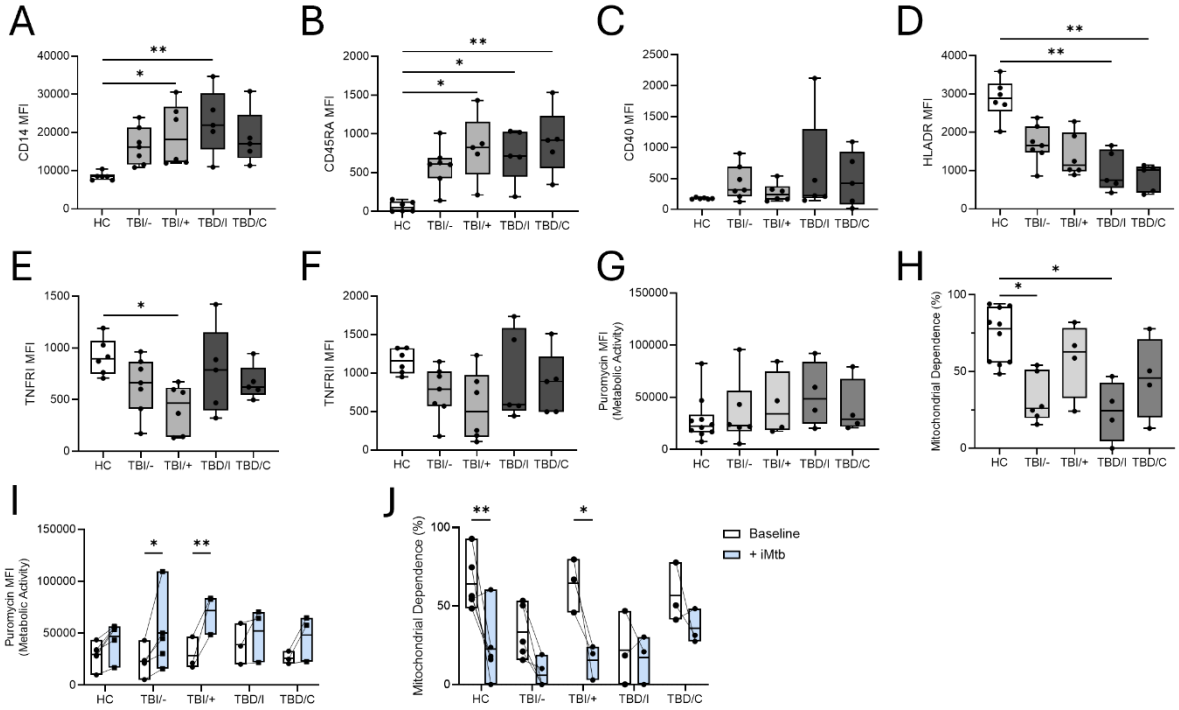
A
CD14 MFI
B
CD45RA MFI
C
CD40 MFI
D
HLADR MFI
E
TNFRI MFI
F
TNFRII MFI
G
Puromycin MFI (Metabolic Activity)
H
Mitochondrial Dependence (%)
I
Puromycin MFI (Metabolic Activity)
J
Mitochondrial Dependence (%)
Baseline
+ iMtb
HC
TBI/-
TBI/+
TBD/I
TBD/C

Figure 5

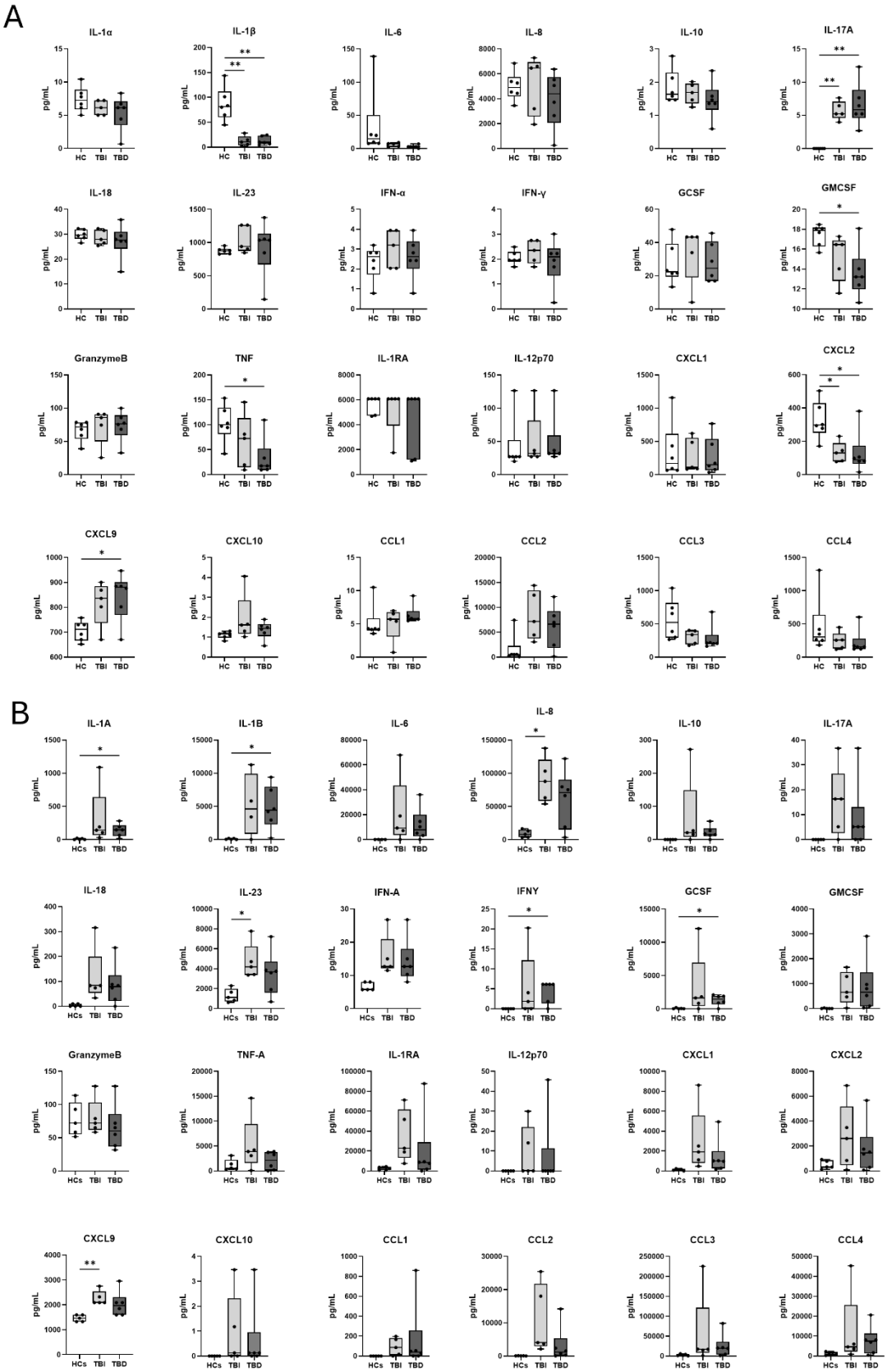
A
IL-1α
IL-1β
IL-6
IL-8
IL-10
IL-17A
IL-18
IL-23
IFN-α
IFN-γ
GCSF
GMCSF
GranzymeB
TNF
IL-1RA
IL-12p70
CXCL1
CXCL2
CXCL9
CXCL10
CCL1
CCL2
CCL3
CCL4
pg/mL
HC
TBI
TBD
B
IL-1A
IL-1B
IL-6
IL-8
IL-10
IL-17A
IL-18
IL-23
IFN-A
IFNY
GCSF
GMCSF
GranzymeB
TNF-A
IL-1RA
IL-12p70
CXCL1
CXCL2
CXCL9
CXCL10
CCL1
CCL2
CCL3
CCL4
pg/mL
HCs
TBI
TBD

660 **Supplemental Figure 1**

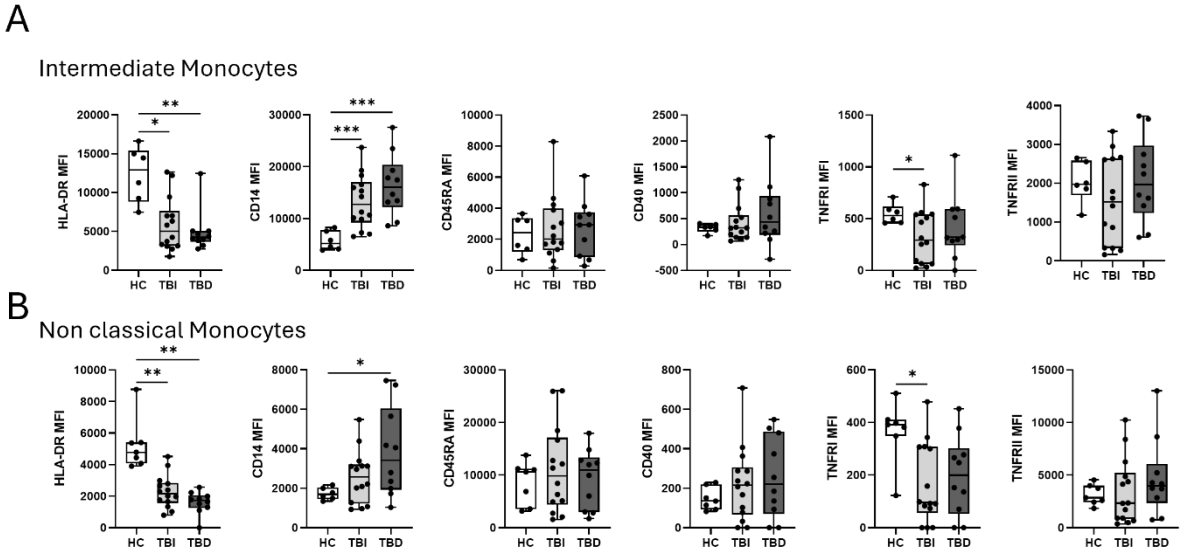

661

662 **Supplemental Figure 2**

663

664